ACOUSTIC IMAGING OF OBJECTS BURIED IN SOIL

*Nail Çadallı *, Catherine H. Frazier **, David C. Munson, Jr. *, William D. O'Brien, Jr. ***

* Coordinated Science Laboratory, ** Bioacoustics Research Laboratory
and Department of Electrical and Computer Engineering
University of Illinois, Urbana, IL, 61801
e-mail: cadalli@csl.uiuc.edu, frazier@ifp.uiuc.edu, d-munson@uiuc.edu, wdo@uiuc.edu

ABSTRACT

A high-resolution acoustic imaging system is proposed for imaging objects buried in soil. The system incorporates a transducer array that collects acoustic data as it is moved across the soil surface. A mathematical model and associated computer software are developed in order to simulate the signals acquired by the actual system. Subsurface images are reconstructed from simulated and real data by using delay-and-sum beamforming and by the application of Synthetic Aperture Radar (SAR) theory to this particular problem.

1. INTRODUCTION

In this study, we propose an acoustic system for high-resolution imaging of objects buried in soil. An acoustic system has potential advantages over other imaging modalities. Ground penetrating radar, for example, can be used only in dry soil. Our application of interest is to detect and image cultural artifacts, which requires much finer resolution than is currently available. Such a system also could be used for other purposes, such as detecting unexploded ordinance.

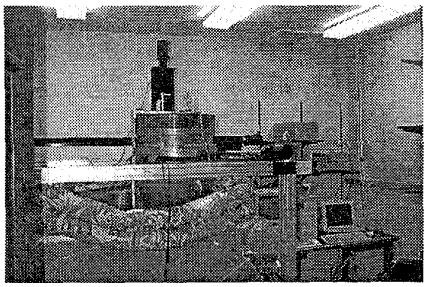

Figure 1: *Experimental system*

This research was supported by the U. S. Army Construction Engineering Research Laboratory under Contract DACA88-96 K 0002.

This paper is organized as follows: In the next section we describe the experimental system. Section 3 introduces the data model. Section 4, explains the methods we use for image reconstruction and presents images reconstructed from both simulated and real data. Finally, we conclude in Section 5.

2. EXPERIMENTAL SYSTEM

We have designed an acoustic imaging system for subsurface imaging that incorporates a torpedo transducer array from the Applied Research Laboratory at Pennsylvania State University. A picture of the system is shown in Figure 1. The soil is contained in a cubic wooden box of 1.2 m on a side. The box has a false bottom, with only the top 60 cm filled with soil. The box is surrounded by a metal frame used to suspend the torpedo head, which contains the receiver array, above the box. The source is to the left of the torpedo. In the picture, the source is connected to the array by a metal arm. This rigid arm was found to couple vibrations from the source to the array and is therefore no longer used for this purpose. Sitting on top of the box of sand is a child's pool filled with water to a depth of 3 cm. The water is used to couple the sound energy between the transducers and the sand. To the right of the frame are two computers. The first is used to control the motion of the receiver array along three translational axes. The second computer controls the data acquisition, including communication with the motion control computer.

The source transducer is a single element that is well approximated as a point source. In future versions of the system, we hope to use a transmitter array to provide focusing of the transmit beam to increase the energy coupled into a localized volume of soil. A 52-element sonar array (8x8, 3.56 cm^2 close-packed elements with 3 elements in each corner missing) serves as the receive array, and allows for beamforming on receive. On receive, the backscattered echo signals from

0-8186-8821-1/98 $10.00 © 1998 IEEE

each of the 52 elements are amplified and digitized. The receiver array and the corresponding coordinate system are shown in Figure 2. The z-axis represents the depth into the soil and the x-y plane represents the soil surface. The y and z dimensions are called *azimuth* and *range*, respectively. The detailed geometry of the transmitter and the receiver is shown in Figure 3. This system has been built and is in operation at the U. S. Army Construction Engineering Research Laboratory (CERL) in Champaign, Illinois, where data are collected from a controlled volume of soil.

3. DATA ACQUISITION MODEL

We have developed a mathematical model and associated computer software to simulate the signals acquired by the above system. Our simulator serves as a convenient platform for the development of image reconstruction algorithms. In our model, the medium (soil) is assumed to consist of densely-spaced point scatterers, which are placed on a three dimensional grid, representing the object(s) and the soil background. Each scatterer is assigned a reflection coefficient $\Gamma_o(x,y,z)$, with $m(x,y,z)$ and $\theta(x,y,z)$ being its magnitude and phase, respectively.

The transmitted signal is a cosine-weighted pulse of 5 cycles at 6 kHz. This frequency has been chosen partly by the operational requirements of the acoustic transducers and partly by resolution considerations. Achievable resolution is determined in part by the medium. Propagation speed determines the wavelength for a given frequency. With a higher frequency, better resolution can be achieved; however, higher frequencies suffer from large attenuation resulting in poor signal-to-noise ratio.

In considering the returned signal, let us first deal with the case of one scatterer. The received response from a particular reflector is a delayed version of the transmitted signal, scaled by the reflection coefficient of the scatterer and by a factor which is dependent on the range function and which is due to the attenuation of the medium and the radial expansion of the spherical wave [1]. The transmitted signal is given as

$$\tilde{s}(t) = \Re e\left\{s(t)e^{j2\pi f_0 t}\right\} \tag{1}$$

where $s(t)$ is a baseband signal of duration T_p.

Receiving element surfaces are considered to be a collection of point receivers. Since the transmitting element is approximately omnidirectional, such a decomposition is not necessary for that element. For a particular scatterer, the signal received at a transducer is the sum of the signals received by those point receivers on the surface of the transducer. This model accounts for the curvature of the wavefront incident on the transducer. The signal received by the i'th receiver from a scatterer at $\mathbf{v} = (x,y,z)$, when the transmitter is at $\mathbf{v}_t = (x_t, y_t, z_t)$ and the center of the receiver array is at $\mathbf{v}_r = (x_r, y_r, z_r)$, is as follows:

$$\begin{aligned}\tilde{g}_i(t,\mathbf{v}_t,\mathbf{v},\mathbf{v}_r) = &\int_{-\infty}^{\infty}\int_{-\infty}^{\infty} w_i(x'',y'';\mathbf{v}_r)m(x,y,z) \\ &\cdot \Re e\left\{s(t-\frac{R_i(\mathbf{\Lambda})}{c})e^{j[2\pi f_0(t-\frac{R_i(\mathbf{\Lambda})}{c})+\theta(x,y,z)]}\right\} \\ &\cdot \frac{e^{-\alpha R_i(\mathbf{\Lambda})}}{\bar{R}(\mathbf{v}_t,\mathbf{v})\bar{R}_i(\mathbf{v}'',\mathbf{v})}dx''dy'' \end{aligned} \tag{2}$$

Here $\mathbf{v}'' = (x'',y'',z'')$ are the coordinates of the simple receiver on the transducer, $w_i(x'',y'';\mathbf{v}_r)$ is the window representing the surface of the i'th receiver when the array center is at $\mathbf{v}_r$, $\mathbf{\Lambda} = [\mathbf{v}\ \mathbf{v}_t\ \mathbf{v}''\ \mathbf{v}_r]$ is defined for notational simplicity, α is the attenuation constant of the medium and c is the speed of sound in soil. The range function $R_i(\mathbf{\Lambda})$ is the sum of $\bar{R}(\mathbf{v}_t,\mathbf{v})$, which is the distance from the transmitter to a particular reflector, and $\bar{R}_i(\mathbf{v}'',\mathbf{v})$, which is the distance from the reflector to the infinitesimal receiver surface on a particular receiver element. The total received signal for a particular location of the receiver array is the sum of responses from all scatterers in the medium. The numerator of the last term in (2) represents the attenuation due to the medium, and the denominator accounts for attenuation due to the spherical expansion of the acoustic wave.

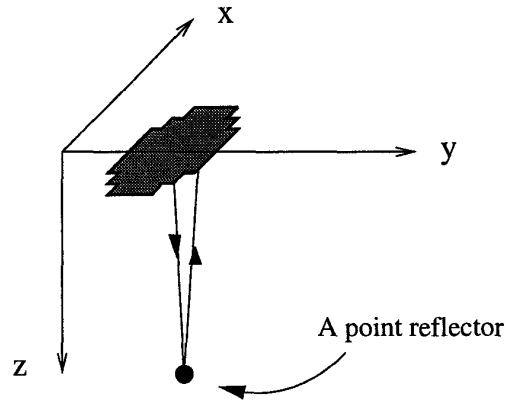

Figure 2: *Array of transducers and associated coordinate system. Surface of the array is in the x-y plane.*

Preliminary to this study, W. D. O'Brien's laboratory evaluated the acoustic propagation properties of six soil types to assess the propagation media's role in imaging subsurface artifacts. The attenuation co-

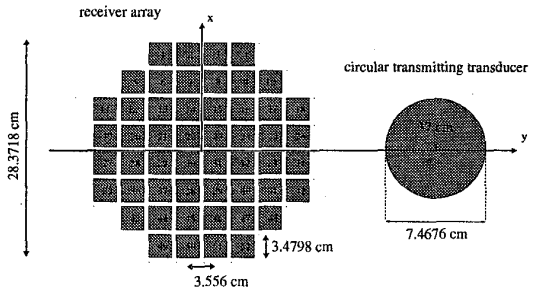

Figure 3: *Geometry of the transmitter and receiving array; view from the top. Origin is at the center of the receiver array.*

efficient in the 1–10 kHz frequency range varied approximately linearly with frequency, and the normalized attenuation coefficient ranged between 0.1 and 1.0 dB/cm-kHz with a mean of approximately 0.5 dB/cm-kHz. The propagation speed ranged from 80 to 250 m/s with values typically in the range from 100 to 200 m/s. Our measured values for speed and attenuation are in the same range as given in the literature [2].

4. IMAGE RECONSTRUCTION

By translating the receiver array across the surface of the medium, it is possible to obtain sufficient data to form an image of the soil subsurface. The data acquisition system is moved along a straight line and at regular spatial intervals the system emits a signal and collects the returns. We mainly have explored two methods of forming images from the collected data, as explained below. Reconstructed images represent the image of $y - z$ plane at a fixed x value according to our coordinate convention in Figure 2.

4.1. Beamforming

At each position of the data acquisition system, a single beam can be formed by focusing the array broadside, so that a conventional B-mode image may be formed. Off-line delay-and-sum beamforming is used to focus the receive beam. Alternatively, since the signals have been recorded separately, several beams can be formed for each source/receiver array position by synthesizing several elements centered at positions between the source and the receiver. To synthesize an element between the source and receiver, the 52 signals are first delayed to simulate a signal transmitted from a synthesized position, and then they are delayed to simulate a focused receiver at the synthesized position. The reason for using such synthesized elements in delay computation rather than using one of the receive elements as a reference to others is to compute the delay for the shortest path length traveled by the transmitted signal for a particular depth so as to reduce the effect of attenuation.

Dynamic focusing is used so that multiple depths in the image are in focus. However, the lateral resolution is still not constant due to the fixed size of the array. The signals present in the final image, whether formed by focusing the beam broadside or by synthesizing several receivers and averaging, are envelope-detected to form the B-mode image. Then a two-dimensional image is formed by displaying the envelope-detected signals side-by-side.

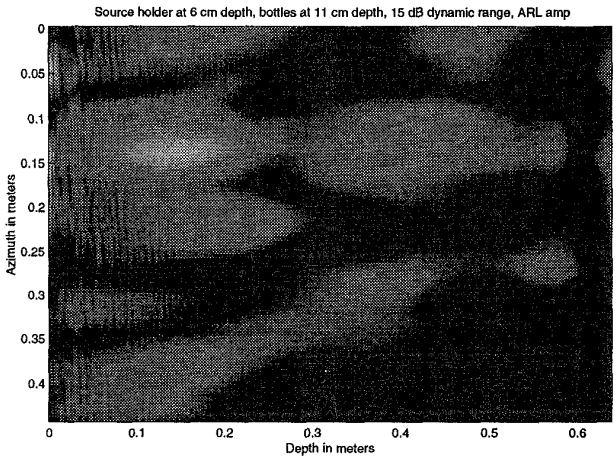

Figure 4: *B-mode reconstructed image of source holder and bottles using real data.*

Figure 4 shows an image reconstructed by using beamforming on real data collected by the experimental system. The soil contained three buried objects: two bottles, and the source holder which is the piece of metal that had been used to connect the source to the receiver array. Although the two ends of the holder have a complicated shape, the center is a bar of metal, $70 \times 10 \times 1$ cm. It was buried 6 cm deep so that the lateral dimension was 1 cm and the axial dimension was 10 cm. The bottles were buried end to end so that at the position where the source and array passed over them, they behaved as an air-filled glass tube, 7 cm in diameter and 30 cm long. They were buried 11.5 cm deep. The data acquisition system was moved in 0.5 cm steps. The image was formed by synthesizing a single element at the position of the receiver array. In this image, the source holder appears as the bright spot at the top left corner of the image. The spot immediately below it is a sidelobe. The spots to the right of the

holder are due to multiple reflections. The bottles appear as a spot at the bottom left corner of the image. We conclude from this image that solid targets give a stronger reflection than air-filled targets do.

One interesting point about the above image is that it was formed using frequency components in a band centered at 600 Hz in the received signals, rather than a band centered at the 6 kHz center frequency. For some reason the low frequency band seems to carry much more information than is present in the carrier frequency band. We are currently working toward a better understanding of this phenomenon.

4.2. SAR Approach

Given N transducers, a linear receiver array could provide far higher resolution than a rectangular array if synthetic aperture processing were used. Suppose data were collected from a linear array moved in a direction normal to its orientation. This corresponds to a linear array with its longer dimension being along the x axis as depicted in Figure 5. High resolution in the direction of travel could then be obtained by using algorithms similar to those employed in synthetic aperture radar (SAR). High resolution along the dimension of the array would be obtained by using the beamforming approaches described above. A difference between subsurface imaging and SAR is that in the former we have attenuation of the signal due to the medium. We have developed a SAR-type reconstruction algorithm for the acoustic imaging scenario using a modification of the correlation algorithm described in [3, 4]. The main steps and the necessary modifications are explained briefly in the following.

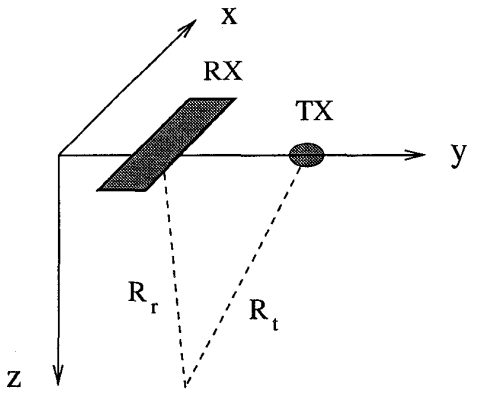

Figure 5: *Linear array and off-center transmitter.*

By passing the returned signal through a quadrature demodulator, the carrier can be suppressed and the complex baseband signal can be obtained for each of the receivers in the linear array. The linear array then can be focused to a fixed depth, or can be dynamically focused to various depths by using beamforming. This results in a single waveform for each location of the data acquisition system. Let us denote the signal obtained after focusing as

$$\bar{g}(t, y_a) = \int_{-\infty}^{\infty}\int_{-\infty}^{\infty} \Gamma_o(y,z) w_a(y-y_a) w_r(z) \cdot s(t - \frac{R_t + R_r}{c}) e^{jk(R_t+R_r)} dy dz \quad (3)$$

where $k = 2\pi f_o/c$ is the wavenumber, and y_a is the azimuth coordinate at which the returns are collected by the linear receiver array. $w_a(y)$ and $w_r(z)$ are window functions representing the area illuminated by the transmitted acoustic beam in the azimuth and range directions, respectively. d is the distance between the transmitter and receiver. First order Taylor approximations of R_r and R_t,

$$R_r = \sqrt{(y-y_a)^2 + z^2} \approx z + \frac{(y-y_a)^2}{2z}$$
$$R_t = \sqrt{(y-y_a-d)^2 + z^2} \approx z + \frac{(y-y_a-d)^2}{2z},$$

are valid if the conditions $z \gg y - y_a$ and $z \gg y - y_a - d$ hold. We assume that the transmitted signal varies slowly enough that $s(t - \frac{R_t+R_r}{c}) \approx s(t - \frac{2z}{c})$. Assigning $\Gamma(y,z) = \Gamma_o(y,z)e^{-j2kz}$ and making the change of variables, $y \to \nu, z \to \xi$, and $t = \frac{2z}{c}$, we can write

$$g(y_a, z) = \int \bar{\Gamma}(y_a, \xi) w_r(\xi) s(\frac{2}{c}(z-\xi)) d\xi \quad (4)$$

$$\bar{\Gamma}(y_a, \xi) = \int \Gamma(\nu, \xi) w_a(\nu - y_a) \exp(-jk\frac{(\nu - y_a)^2}{2\xi}) \cdot \exp(-jk\frac{(\nu - y_a - d)^2}{2\xi}) d\nu \quad (5)$$

In the so-called range processing step, the received signal in (4) is correlated with the transmitted signal to find an estimate for $\bar{\Gamma}(y_a, z)$. Then this estimate is used to solve for $\Gamma(y_a, z)$ by correlating $\bar{\Gamma}(y_a, z)$ with the filter having the linear phase terms in (5). This step is called azimuth processing. With the above formulation, range processing is the same as in the standard correlation-based SAR algorithm in [3]. But in the standard algorithm, since it has been derived for a radar scenario, there is only one signal received by the single antenna located on the radar platform. Also, for the case of a single antenna, the transmitter-to-reflector and reflector-to-receiver distances are the same in the radar case. Notice that the attenuation term in (2) is

not incorporated in (3). This is because we apply time-gain compensation to the received signal to compensate approximately for the effect of attenuation.

The above SAR-type algorithm was applied to simulated data consisting of three point targets. Only the linear array of 8 receivers at the center of the receiver array were used. The point targets were positioned at $x = y = 0$ and at depths 0.1 m, 0.4 m, 0.7 m. The resulting image is shown in Figure 6. We used time-gain compensation to eliminate the effect of attenuation to some extent. Without the compensation, only the scatterer at $z = 0.1$ could be seen. Note that the point objects are not reconstructed at their correct locations. This effect is most noticeable for the object closest to the surface. The reason for this is that our Taylor approximations for the transmitter-reflector-receiver distances are not valid for close objects. In a SAR scenario, these approximations generally are valid because the range distance in radar imaging is typically very large. Note also that we approximated two distance functions in our case to take into account the off-center transmitter. If the standard monostatic SAR algorithm had been applied without that modification, the point target images in Figure 6 would have been shifted in azimuth direction, too.

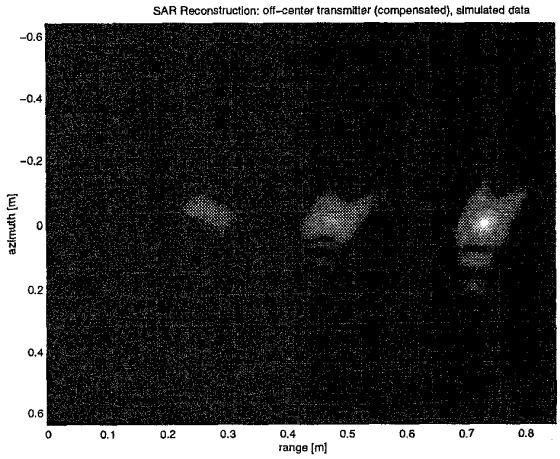

Figure 6: *SAR-type reconstruction of three point sources from simulated data .*

To eliminate problems due to the range approximations, we are currently implementing another SAR-type algorithm, namely, the $w - k$ algorithm, which is expected to give more accurate results for near-field sources [5, 6].

In a SAR reconstruction, resolution in the range direction increases as the bandwidth of the transmitted signal increases. Azimuth resolution depends on the distance covered by the data acquisition system during illumination of a target by the transmitted acoustic beam. Collecting more data in the azimuth dimension provides for an increase in resolution in the azimuth direction. In our experimental system, we are limited by the controlled volume of soil, which presents a complication to successfully applying SAR-type imaging to our experimental data.

5. CONCLUSION

An acoustic approach was described for imaging objects buried in soil, with the primary purpose of detecting and imaging cultural artifacts. An experimental system was designed and implemented. Also, a mathematical model and associated computer software were developed in order to simulate the signals acquired by the actual system. Subsurface images were reconstructed from real and simulated data by using delay-and-sum beamforming and by the application of synthetic aperture theory. Our preliminary experimental results showed that the detection of objects is possible, but that further improvements may be necessary to image objects in significant detail.

6. REFERENCES

[1] Allan D. Pierce. *Acoustics: An Introduction to Its Physical Principles and Applications.* McGraw-Hill, 1981.

[2] C.J. Hickey and J.M. Sabatier. Measurements of two types of dilatational waves in an air-filled unconsolidated sand. *J. Acoust. Soc. Am.*, 102(1):128–136, July 1997.

[3] David C. Munson Jr. and Robert L. Visentin. A signal processing view of strip-mapping synthetic aperture radar. *IEEE Trans. Acoust., Speech, Signal Processing*, 37(12):2131–2147, December 1989.

[4] John C. Curlander and Robert N. McDonough. *Synthetic Aperture Radar.* Wiley Series in Remote Sensing. John Wiley & Sons, 1991.

[5] C. Cafforio, C. Prati, and F. Rocca. SAR data focusing using seismic migration techniques. *IEEE Trans. Aerospace and Electronic Systems*, 27:194–207, March 1991.

[6] M. Soumekh. A system model and inversion for synthetic aperture radar imaging. *IEEE Trans. Image Processing*, 1:64–76, Jan. 1992.